

NJC

Accepted Manuscript



This is an *Accepted Manuscript*, which has been through the Royal Society of Chemistry peer review process and has been accepted for publication.

Accepted Manuscripts are published online shortly after acceptance, before technical editing, formatting and proof reading. Using this free service, authors can make their results available to the community, in citable form, before we publish the edited article. We will replace this *Accepted Manuscript* with the edited and formatted *Advance Article* as soon as it is available.

You can find more information about *Accepted Manuscripts* in the [Information for Authors](#).

Please note that technical editing may introduce minor changes to the text and/or graphics, which may alter content. The journal's standard [Terms & Conditions](#) and the [Ethical guidelines](#) still apply. In no event shall the Royal Society of Chemistry be held responsible for any errors or omissions in this *Accepted Manuscript* or any consequences arising from the use of any information it contains.



Journal Name

ARTICLE

Hierarchically Porous Titanium Phosphate Monoliths and Its Crystallization Behavior in Ethylene Glycol

Received 00th January 20xx,
Accepted 00th January 20xx

DOI: 10.1039/x0xx00000x

www.rsc.org/

Yang Zhu,^a Koji Yoneda,^a Kazuyoshi Kanamori,^a Kazuyuki Takeda,^a Tsutomu Kiyomura,^b Hiroki Kurata^b and Kazuki Nakanishi^{*a}

Hierarchically porous titanium phosphate monoliths combining well-defined co-continuous macropores and accessible large mesopores have been for the first time synthesized via sol-gel process accompanied by phase separation using titanium oxysulfate and phosphoric acid as precursors. The macropore size was tunable over a broad range from 0.6 μm to 10 μm by changing the starting composition, while the mesopore size and the specific surface area of the as-synthesized amorphous monolith are 21 nm and 320 m^2g^{-1} , respectively. Crystallization of the gel network can be induced in two different ways. Calcination at elevated temperature (800 $^\circ\text{C}$) leads to the formation of TiP_2O_7 and the collapse of both the macro and meso structures, while solvothermal treatment of the as-synthesized gel in ethylene glycol leads to the formation of platy crystals of titanium phosphate with layered structure at relatively low temperature. The titanium phosphate monolith with hierarchically porous structure is expected to be useful in various applications such as continuous-flow catalysis, water remediation and ion batteries.

Introduction

Hierarchically porous monolithic materials combining both nanometer level micro/mesopores and micrometer level macropores are attracting increasing attentions from both academic and industrial perspectives¹. In addition to the common features of porous materials such as high surface area and pore volume, this category of materials stands out for their excellent flow-through properties ensuring good access to the reactive surfaces, as well as the ease for reuse and recycle which are preferable for industrial production. Although the methods for mesostructure fabrication have been developed for long, approaches for the introduction of macropores into monoliths are still limited and the control over detailed pore parameters remains challenging by conventional processing routes for macroporous ceramics such as templating and direct foaming². One of the recently developed methods for the synthesis of macroporous monoliths with controlled pore parameters is those using macroscale phase separation that falls in spinodal decomposition region, which often leads to a three-dimensionally connected (co-continuous) macroporous

structure³. The mesostructure embedded in the macroscale skeletons are either from the interstitial of the constituent colloidal particles or from the removal of the nanoscale template such as self-assembled block copolymers. Mesopore characteristics can thus be tailored either by the deliberate control of particle size or by the control of structures and properties of the template. Hence, such synthetic method enables the independent control of macro and mesoscale morphologies. Since the first success on silica⁴, the applicability of this method has been extended over a broad range of materials, such as metal oxides (titania⁵, zirconia⁶, alumina⁷, iron oxide⁸, etc.), mixed oxides (zinc ferrite⁹, mullite¹⁰, layered double hydroxide¹¹), metal phosphates (calcium phosphate¹², lithium iron phosphate¹³, aluminum phosphate¹⁴, zirconium phosphate¹⁵), hybrid polysiloxane compounds¹⁶⁻¹⁸ as well as polymers¹⁹⁻²¹. The hierarchically porous monoliths thus obtained are used for different applications such as chromatographic separations²², ion sorptions^{15,23}, lithium ion batteries¹³ and continuous-flow catalysis²⁴.

Shaping metal(IV) phosphates, a well-known family of layered compounds, into hierarchically porous monoliths will further extend their applications as catalysts and ion sorbents. The difficulty in obtaining a homogeneous gel as compared with the cases of other metal phosphates and oxides, however, lies in the high coordination number of tetravalent metal and large number of coordination sites in phosphoric acid and the high lattice energy of the resultant metal(IV) phosphate. The mixture of metal(IV) species and phosphoric acid in aqueous medium often leads to instant polycondensation and prompt crystallization, resulting in sedimentation of precipitates.

^a Department of Chemistry, Graduate School of Science, Kyoto University, Kitashirakawa, Sakyo-ku, Kyoto, 606-8502, Japan.
E-mail: kazuki@kuchem.kyoto-u.ac.jp

^b Institute for Chemical Research, Kyoto University, Uji, 611-0011, Japan.

Electronic Supplementary Information (ESI) available: FE-SEM images of TP monoliths synthesized with and without the addition of DMSO, Raman spectrum of the sample TP-0-0, ³¹P NMR of TP monolith calcined at 600 $^\circ\text{C}$, N₂ adsorption-desorption isotherms, BJH pore size distributions, calculated detailed pore parameters and compositional information from EDX measurement of calcined TP monoliths and solvothermally treated TP monoliths. See DOI: 10.1039/x0xx00000x

Hence, a deliberately controlled condensation kinetics between metal(IV) aquo complex and phosphoric acid is highly desirable to reach a structurally stable monolith and a success has been achieved only in zirconium phosphate as the first example. Titanium phosphates (TP) as another well-known metal(IV) phosphate, due to its diversity in composition and crystal structure, show high potentials for applications in different fields ranging from cosmetics²⁵ to catalysis²⁶ and solar cells²⁷. In this research, hierarchically porous TP monoliths have been synthesized via sol-gel process accompanied by phase separation. The macropore size can be controlled by adjusting the amount of polymers as phase separation inducers, and large mesopores are derived from interstitials of particles constituting the macroscale skeletons. Crystallization of as-synthesized amorphous TP monoliths has been investigated either by heat treatment at elevated temperature or by solvothermal treatment in ethylene glycol. The latter process leads to the formation of layered nanosheets with the original macroporous morphology being preserved.

Experimental

Reagents

Titanium(IV) oxysulfate ($\text{TiOSO}_4 \cdot x\text{H}_2\text{O}$, Sigma-Aldrich Co., USA) and concentrated phosphoric acid (≥ 85 wt% in H_2O , Sigma-Aldrich Co., USA) were respectively used as sources of titanium and phosphate. A mixture of distilled water (Hayashi Pure Chemical Ind., Co., Ltd., Japan), glycerol (Kishida Chemical, Japan), and dimethyl sulfoxide (DMSO, Kishida Chemical, Japan) were used as the solvent. Poly(ethylene oxide) (PEO, average molecular weight 100 000, Sigma-Aldrich Co., USA) and polyvinylpyrrolidone (PVP, average molecular weight 55 000, Sigma-Aldrich Co., USA) were used as the phase separation inducers. Both 2-propanol and ethylene glycol (EG) (Kishida Chemical, Japan) were used as the solvents for solvent exchange of the wet gels, while EG was further used for solvothermal treatment. All reagents were of analytical grade and used as received without further purification.

Synthesis of hierarchically porous TP monolith

TP monoliths were prepared with the following procedure; 0.64 g of titanium oxysulfate and predetermined amounts of PEO and PVP were dissolved in the mixed solvent of 1 mL of water, 1.0 g of glycerol, and 0.4 mL of DMSO. The mixture was stirred until a homogeneous solution was obtained. The solution was then cooled to 0 °C in an ice-water bath, followed by the addition of 0.55 mL of 0 °C cooled concentrated phosphoric acid (molar ratio of P / Ti is 2). The resultant solution was stirred vigorously for 1 min, degassed in ultrasonic bath for 10 s and subjected to gelation at 0 °C. After gelation, the wet gel was aged at room temperature for 24 h, and solvent-exchanged with 2-propanol for 3 times (more than 12 h per each time). The resultant wet gel was dried slowly first at room temperature, then at 40 °C and 60 °C in order to obtain crack free dried monolith. The time spent for drying at

each temperature was 24 h. The obtained gel was denoted as TP-x-y, where x and y represents the amount of PEO and PVP respectively.

Solvothermal treatment of TP monolith

TP-0.05-0.08 was chosen as the standard sample for solvothermal treatment in EG. In a typical run, a TP monolith with its mother liquor being thoroughly exchanged with 2-propanol was immersed in EG at room temperature for more than 24 h. The volume of EG used for solvent exchange and solvothermal treatment was 20 times of the bulk volume of the gel. The TP monolith exchanged with EG was then transferred to a Teflon liner filled with EG, sealed in a stainless autoclave and subjected to solvothermal treatment for 24 h. The resultant gel was then solvent-exchanged again with sufficient amount of 2-propanol for 3 times and dried at 60 °C for more than 3 d.

Characterization

Morphology of the fractured surface of the samples and the chemical compositions were investigated by scanning electron microscopy-energy dispersive X-ray spectroscopy (SEM-EDX, JSM-6060S equipped with JED-2300, JEOL, Japan), field emission scanning electron microscopy (FE-SEM, JSM-6700F, JEOL, Japan) and transmission electron microscopy (TEM, JEM-2200FS, JEOL, Japan) equipped with a spherical aberration corrector (CEOS, CETCOR, Germany). The crystal structure was confirmed by powder X-ray diffraction (XRD, RINT Ultima III, Rigaku Co., Japan) using $\text{Cu K}\alpha$ ($\lambda = 0.154$ nm) as an incident beam. Thermal properties of the samples were investigated by thermogravimetry-differential thermal analysis (TG-DTA, Thermal Plus TG 8120, Rigaku Co., Japan) with a continuous air supply at 100 mL/min. Fourier transform infrared spectroscopy (FT-IR, IR Affinity-1, Shimadzu Co., Japan), Raman spectroscopy (XploRA, HORIBA, Ltd., Japan) and elemental analysis were performed to confirm the molecular and atomic level information. The molecular-level environments of phosphorus in the monolith were measured by solid-state ^{31}P single pulse magic angle spinning nuclear magnetic resonance (MAS NMR) performed at room temperature in a magnetic field of 7 T on an OPENCORE NMR spectrometer^{28,29} with a 5 mm MAS probe. The carrier frequency for ^{31}P was 121.24913 MHz and the sample spinning frequency was 9.2 kHz for as-synthesized sample and 10 kHz for the calcined and the solvothermally treated samples. For each sample, signals were accumulated over 100 times with a repetition period of 100 s. Meso- and microstructure of the samples were characterized by nitrogen adsorption-desorption measurement (BELSORP-mini II, Bel Japan Inc., Japan).

Results and discussion

Synthesis of hierarchically porous TP monolith

In our previous research, glycerol has been found to be effective in controlling the kinetics of the condensation between metal aquo complex and phosphoric acid in the sol-

gel synthesis of zirconium phosphate monolith¹⁵. The coordination effect of the hydroxyl groups to the metal aquo complex provides spatial hindrance while the high viscosity limits mass transfer in the solution. Similarly during the synthesis of TP monoliths, only precipitates were obtained in the absence of glycerol in the starting composition. However, the suppression effect on crystal growth of TP was still not strong enough only by the addition of glycerol (Figure S1A, where platy particles and spherical particles of larger size were observed), and as a result, the mechanical strength of the obtained gel was still friable. The coordination effect between DMSO and tetravalent metals such as Ti, Zr, Sn is also well known and commonly used for the synthesis of metal phosphonates³⁰⁻³². Therefore DMSO was added to further suppress the particle growth by the stronger coordination between the sulfoxy group and titanium aquo complex. The smaller particle size leads to more interfaces among the particles (Figure S1B), which thus increased the mechanical strength of the obtained gel. The incorporation of DMSO via its coordination to the TP gel network was confirmed by resolved characteristic Raman absorbance bands in the Raman spectrum of TP-0-0 at 682, 720, 2930, 3011 cm^{-1} , which shift from the original bands of DMSO at 670, 700, 2919, 2997 cm^{-1} (Figure S2)³³.

In our previous research, the addition of a combination of

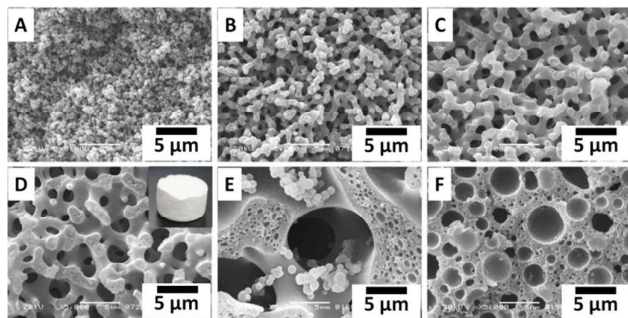


Figure 1 SEM images of TP monoliths synthesized with different amounts of PVP; TP-0.05-0 (A), TP-0.05-0.04 (B), TP-0.05-0.06 (C), TP-0.05-0.08 (D) (inset shows the appearance of the sample TP-0.05-0.08), TP-0.05-0.12 (E) and TP-0.05-0.16 (F).

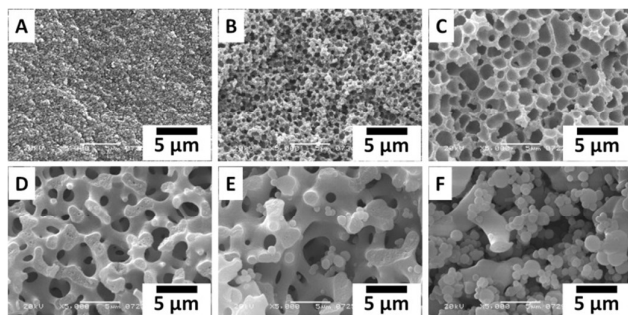


Figure 2 SEM images of TP monoliths synthesized with different amounts of PEO; TP-0-0.08 (A), TP-0.01-0.08 (B), TP-0.03-0.08 (C), TP-0.05-0.08 (D), TP-0.07-0.08 (E) and TP-0.1-0.08 (F).

water-soluble polymers, such as polyacrylamide / PEO¹⁵, PVP / PEO¹³ was proven to be effective in inducing controlled phase separation in metal phosphate systems, whereas inducing phase separation was difficult with a single polymer. In SEM images in Figure 1 and Figure 2, the effect of the amount of added polymers (PVP and PEO) on the macroscopic structure of the obtained TP monoliths is shown. When only PEO was added, a monolith with submicrometer-sized macropores was obtained. As the amount of PVP was increased with a fixed amount of PEO, monoliths with co-continuous macroporous structure were successfully obtained with the average macropore size ranging from 0.6 to 10 μm (Figure 1B-E), while an excessive amount of PVP led to a monolith with isolated macropores (Figure 1F). PVP is deduced to be preferentially distributed to the gel-rich phase in a two-phase system via the coordination between amide groups and the TP oligomers, which is similar to the case of our previously reported sol-gel system of lithium iron phosphate¹³. Therefore the increase of the amount of PVP subsequently leads to the increased volume fraction of the gel-rich phase in the system. Hence, at excessive amount of PVP, morphology with isolated macropores was obtained. Meanwhile, the interaction between PVP and polymerizing TP oligomers results in a relatively hydrophobic PVP-TP composite, which thus decreases the compatibility between the polar solvent and the gel network consisting mainly of such composites, leading to higher phase separation tendency. On the contrary, PEO is deduced to be preferentially distributed to the solvent-rich phase. When only PVP was added, a translucent gel without micrometer-sized macropores was obtained (Figure 2A). The addition of small amount of PEO together with PVP gave rise to the gels with isolated macropores (Figure 2B, C), due to the relatively large volume fraction of the gel-rich phase containing PVP. The increase in the amount of PEO increased the volume fraction of the solvent-rich phase, leading to the formation of co-continuous macropores and further to aggregates of microspheres when the amount was excessive. In the meantime, the increase in the content of PEO in the solvent-rich phase enhanced the phase separation tendency due to the decreasing compatibility between the PVP-containing gel-rich phase and PEO-containing solvent-rich phase. Consequently, when a small amount of PEO was added, structure with isolated macropores was obtained and the increase of PEO amount led to increased macropore size. Similarly at relatively higher PEO content, the increase of the amount of PEO led to the increase of the size of co-continuous macropores (Figure 2D, E). Overall, with an appropriate amount of polymers in the starting composition, monolithic TP gel with well-defined co-continuous macroporous morphology of controlled macropore size can be obtained.

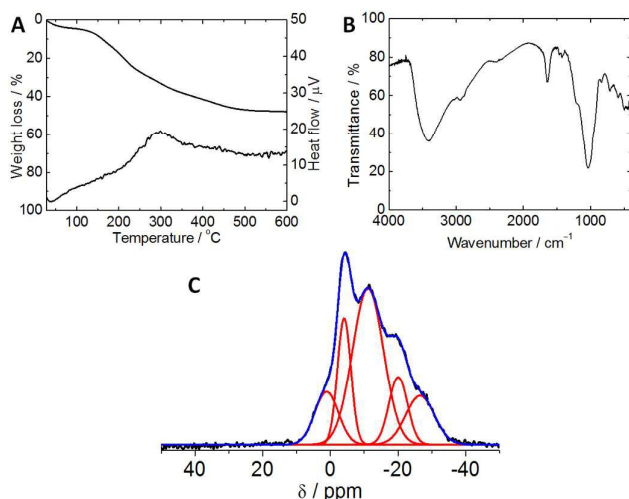


Figure 3 TG-DTA curves (A), FT-IR spectrum (B) and ^{31}P NMR spectrum (C) of TP-0.05-0.08 (black curve: original data, red curve: fitting peaks of the original data, blue curve: peak sum of fitting peaks).

Detailed compositional information on the TP monolith was revealed by EDX, elemental analysis, FT-IR, TG-DTA and ^{31}P NMR and the results are shown in Figure 3 and Table S1. From EDX measurement, the molar ratio of P:Ti in the as-synthesized TP-0.05-0.08 gel is 2.1, slightly higher but very close to that of both precursors added in the starting composition. The incorporation of PVP in the gel network is revealed by elemental analysis with 1.1 wt% of N in the as-synthesized gel. Such result is further confirmed from TG-DTA curves with a broad exothermic peak and the corresponding weight loss at 300 °C due to the combustion of PVP. The strong absorption band at 1030 cm^{-1} and two close absorption bands at 2941 cm^{-1} and 2880 cm^{-1} in FT-IR are attributed to the stretching vibration of phosphate groups bonded to Ti and the vibration of C-H bond in the organic species incorporated in the gel network, respectively³⁴. Besides, the presence of large amount of S (molar ratio of S/Ti as 0.53, 4.9 wt%) in the as-synthesized gel is revealed, which is mainly derived from the incorporation of DMSO in the gel network. The ^{31}P NMR spectrum revealed the complexity of the chemical environment of P in the gel network due mainly to the amorphous structure and the incorporation of different organic species. After applying fitting to the original spectrum, in total 5 resolved peaks were observed, featuring respectively at 0, -4.1, -11.2, -20.0, -27.0 ppm. The chemical shift at 0 ppm can be assigned to the adsorbed phosphoric acid in the gel network. As is revealed from the previous study of ^{31}P NMR spectra of titanium phosphate, the increase of connectivity commonly leads to an upfield shift for the resonance peak³⁵. Based on the phosphorous chemical shift data for $\text{Ti}(\text{OH})(\text{H}_2\text{PO}_4) \cdot 2\text{H}_2\text{O}$ ³⁶ and $\text{Ti}_2\text{O}_3(\text{H}_2\text{PO}_4)_2 \cdot 2\text{H}_2\text{O}$ ³⁷, the chemical shift at -4.1 ppm and -11.2 ppm can be assigned to poorly connected and well connected H_2PO_4^- groups, respectively, while the chemical shifts at -20 ppm and -27 ppm can be assigned to HPO_4^{2-} and PO_4^{3-} considering the ^{31}P

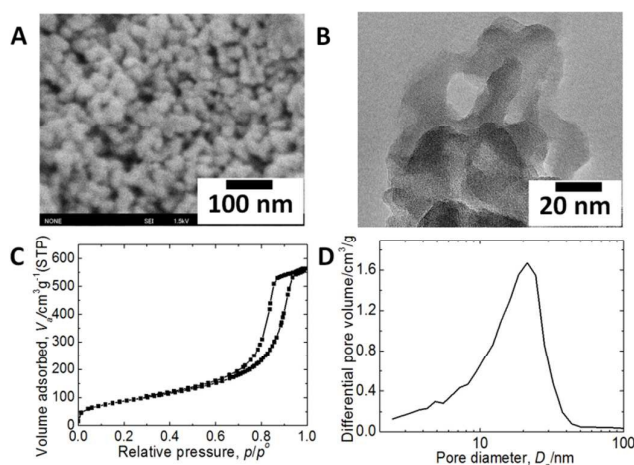


Figure 4 FESEM image (A), TEM image (B) and N_2 adsorption-desorption isotherm (C) and BJH mesopore size distribution obtained from the adsorption branch (D) of TP-0.05-0.08.

NMR spectrum of α -TP ($\text{Ti}(\text{HPO}_4)_2 \cdot \text{H}_2\text{O}$)³⁸ and π/ρ -TP ($\text{Ti}_2\text{O}(\text{PO}_4)_2 \cdot 2\text{H}_2\text{O}$)³⁴.

The skeleton of the obtained macroporous gel was found consisting of particles of 20-30 nm, the interstices of which are the origin of mesopores (Figure 4A). Similar results were observed from TEM images, revealing the amorphous nature of TP particles and showing that the mesopores are of the similar size range as that of the particles (Figure 4B). The presence of mesopores was further confirmed by N_2 sorption isotherm with the BET specific surface area as 320 $\text{m}^2 \text{g}^{-1}$ (Figure 4C). The distribution of mesopore size was calculated ranging from 4 nm to 40 nm with the average as 21 nm from the adsorption branch by the BJH method (Figure 4D). To the best of our knowledge, such TP materials with relatively high surface area and large mesopores (more than 10 nm) are rare among synthesized TP materials, let alone a monolithic form embedded with accessible macro/mesoporous structure, which is highly promising to be used as sorbent, catalyst and catalyst support for various applications.

Effect of heat treatment

The thermal stability of the porous morphology and the

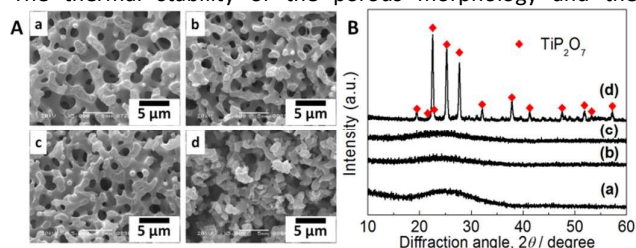


Figure 5 SEM images (A) and XRD patterns (B) of as-synthesized TP-0.05-0.08 (a) and TP-0.05-0.08 calcined at different temperatures, 600 °C (b), 700 °C (c) and 800 °C (d).

subsequent crystal structure change were investigated and the results are shown in Figure 5. Macroporous structure with slightly smaller skeleton size was obtained after calcination at 700 °C. Judging from the TG curve, organic species were totally removed after calcination at 600 °C (Figure 3B). Only two resonance peaks featuring at -22.8 ppm and -33.5 ppm were observed in the ^{31}P NMR spectrum of the sample calcined at 600 °C, and the peaks can be assigned to HPO_4^{2-} and PO_4^{3-} groups (Figure S3)^{34,35}, indicating the condensation of the -Ti-OH and -P-OH groups during the calcination process accompanied by shrinkage of the gel skeletons. Since the mesopore size is relatively large, the condensation imposed little influence on the mesopore size but significantly decreased the volume fraction contributed from micropores and smaller mesopores, leading to the sharper mesopore size distribution as shown in Figure S4B. A further increase in the calcination temperature to 800 °C led to the total dehydration of phosphate groups into pyrophosphate groups, giving the crystal phase of TiP_2O_7 . Such crystallization behavior deteriorated the macroporous as well as the mesoporous structure (Figure 5A-d, Figure S4).

Crystallization behavior of TP monolith in EG

The phase transition behavior from amorphous intermediates to crystalline analogues is commonly found in inorganic materials. Compounds containing cations with moderate charge densities such as Ca^{2+} or Zn^{2+} , due to their possibility to reversibly bind water molecules, are used as guidelines to illustrate nonclassical crystallization behaviors^{39,40}. Calcium phosphate and zinc phosphate, due to their biomedical importance, are perhaps studied the most among phosphate materials^{41,42} for their phase transition. Though, less is known about the crystallization behavior in inorganic metal(IV) phosphates. Herein we found that the crystallization of amorphous TP occurs in EG under solvothermal condition.

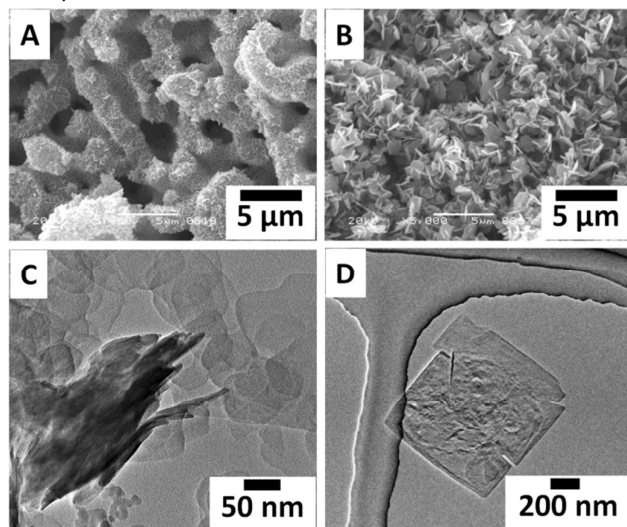


Figure 6 SEM images and TEM images of TP-0.05-0.08 after solvothermal treatment in EG at different temperatures, 100 °C (A, C) and 200 °C (B, D) for 24 h.

After solvothermal treatment at 100 °C for 24 h, the original globular nanoparticles (20-30 nm in diameter, Figure 4A, B) transformed into nanosheets (50-100 nm in diameter, less than 10 nm in thickness), while the original macroporous morphology remained unchanged (Figure 6A, C). Such morphological change led to the increase of mesopore size from 21 nm to 66 nm (Figure S5). Increase of temperature for the treatment to 200 °C enhanced the particle growth kinetics, leading to larger-sized (about 1 µm) square-shaped nanosheets, which though deteriorated the original macroporous morphology (Figure 6B, D). The XRD results in Figure 7A show one resolved diffraction peak at 28.10° and a broad one centered at 10.36°, indicating the average interlayer distance as 0.854 nm with considerable disorder in the interlayer spacing for the sample treated at 100 °C. For the sample treated at higher temperature, the diffraction peak at low angle became sharper and stronger and shifted to 11.96°, implying more ordered interlayer spacing in a longer range, which is consistent with the results from SEM and TEM images that show larger-sized platy crystals (Figure 7B, D). Likewise, the diffraction peak at high angle shifted to 28.30°. However, the peak intensity as well as the sharpness remained similar to that of the sample treated at 100 °C. The effect of temperature of solvothermal treatment can be explained by two essential kinetics of crystallization from the dissolved amorphous TP particles during the solvothermal treatment, namely the nucleation (atomic scale) and growth (alignment of layered structural units) of platy crystals, the former being less temperature dependent in sufficiently supersaturated conditions. Though some other small diffraction peaks are also observed, the presence of only two resolved diffraction peaks strongly indicates the presence of poorly crystalline or even amorphous domains in the nanosheets. Such speculation is further supported by the ^{31}P NMR result in Figure 7B. The peaks at various chemical shifts reveal the complexity of the chemical environment for P even in the sample solvothermally treated at 200 °C. No S and N were detected by elemental analysis, indicating the total removal of PVP and DMSO incorporated in TP network after solvothermal treatment at 200 °C and leading to a compositionally purer TP gel. However, the loss of P was

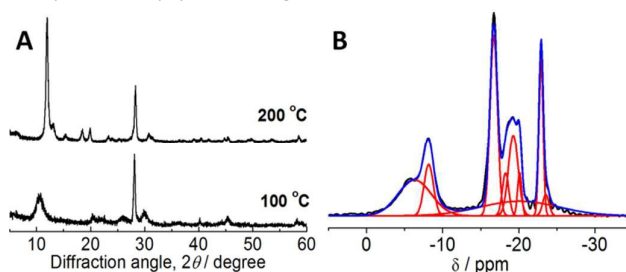


Figure 7 XRD patterns of TP-0.05-0.08 after solvothermal treatment in EG at different temperatures for 24 h (A) and ^{31}P NMR spectrum of TP-0.05-0.08 after solvothermal treatment in EG at 200 °C for 24 h (B, black curve: original data, red curve: fitting peaks of the original data, blue curve: peak sum of fitting peaks).

observed as a result of the crystallization process during the solvothermal treatment (Table S1). Though the detailed mechanism is still unclear, the results obtained and information revealed here will offer insights for the clarification of the crystallization process of amorphous TP in EG.

Conclusions

Detailed synthetic conditions for hierarchically porous TP monoliths and the mechanism for porous structure formation are studied. The incorporation of both glycerol and DMSO in the gel network via coordination successfully suppresses the otherwise heterogeneous polymerization of titanium phosphate network and leads to the formation of monolithic gel consisting of smaller TP nanoparticles, the interstitials of which are the origin of relatively large mesopores (21 nm). The polymers PEO and PVP behave as phase separation inducers, which are responsible for the formation of co-continuous macroporous morphology. Macroporous structure is stable against heat treatment up to 700 °C. The condensation during the process eliminates micropores and smaller mesopores, while imposing negligible effects on the median mesopore size. Pure TiP_2O_7 phase is obtained at 800 °C, which though leads to densification of the gel skeletons and the deterioration of the macroporous morphology. An alternative way for the crystallization of the starting amorphous gel network is by solvothermal treatment in EG, which transforms the amorphous globular TP nanoparticles into layered nanosheets. The control of nanosheet size can be achieved by changing the temperature of the solvothermal treatment. At 100 °C, the starting macroporous structure is maintained, while the growth of nanocrystal blocks the macropores at 200 °C. Such phenomenon is for the first time observed in TP systems and the detailed mechanism is currently under investigation. The hierarchically porous TP monolith with controlled crystallinity is highly promising to be applied in various fields such as water remediation and continuous flow heterogeneous catalysis.

Acknowledgements

The present work was financially supported by the Advanced Low Carbon Technology Research and Development Program (ALCA) from the Japan Science and Technology Agency (JST) and JSPS KAKENHI Grant Number 15J00156.

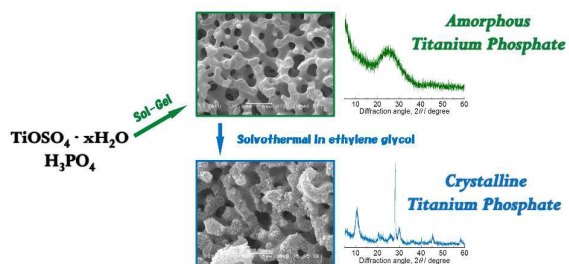
Notes and references

- B. L. Su, C. Sanchez, X. Y. Yang, Hierarchically Structured Porous Materials: From Nanoscience to Catalysis, Separation, Optics, Energy, and Life Science, Wiley-VCH, Weinheim, 2012.
- A. R. Studart, U. T. Gonzenbach, E. Tervoort, L. J. Gauckler, *J. Am. Ceram. Soc.*, 2006, **89**, 1771.
- K. Nakanishi, *J. Porous Mater.*, 1997, **4**, 67.
- K. Nakanishi, Y. Sagawa, N. Soga, *J. Non-Crystalline Solids*, 1991, **134**, 39.

- J. Konishi, K. Fujita, K. Nakanishi, K. Hirao, *Chem. Mater.*, 2006, **18**, 6069.
- J. Konishi, K. Fujita, S. Oiwa, K. Nakanishi, K. Hirao, *Chem. Mater.*, 2008, **20**, 2165.
- Y. Tokudome, K. Fujita, K. Nakanishi, K. Miura, K. Hirao, *Chem. Mater.*, 2007, **19**, 3393.
- Y. Kido, K. Nakanishi, A. Miyasaka, K. Kanamori, *Chem. Mater.*, 2012, **24**, 2071.
- Y. Kido, K. Nakanishi, K. Kanamori, *RSC Adv.*, 2013, **3**, 3661.
- X. Guo, W. Li, K. Nakanishi, K. Kanamori, Y. Zhu, H. Yang, *J. Eur. Ceram. Soc.*, 2013, **33**, 1967.
- Y. Tokudome, N. Tarutani, K. Nakanishi, M. Takahashi, *J. Mater. Chem. A*, 2013, **1**, 7702.
- Y. Tokudome, A. Miyasaka, K. Nakanishi, T. Hanada, *J. Sol-Gel Sci. Technol.*, 2011, **57**, 269.
- G. Hasegawa, Y. Ishihara, K. Kanamori, K. Miyazaki, Y. Yamada, K. Nakanishi, T. Abe, *Chem. Mater.*, 2011, **23**, 5208.
- W. Li, Y. Zhu, X. Guo, K. Nakanishi, K. Kanamori, H. Yang, *Sci. Technol. Adv. Mater.*, 2013, **14**, 045007.
- Y. Zhu, T. Shimizu, T. Kitashima, K. Morisato, N. Moitra, N. Brun, K. Kanamori, K. Takeda, M. Tafu, K. Nakanishi, *New J. Chem.*, 2015, **39**, 2444.
- K. Nakanishi, K. Kanamori, *J. Mater. Chem.*, 2005, **15**, 3776.
- K. Kanamori, K. Nakanishi, *Chem. Soc. Rev.*, 2011, **40**, 754.
- N. Moitra, K. Kanamori, T. Shimada, K. Takeda, Y. H. Ikuhara, X. Gao, K. Nakanishi, *Adv. Funct. Mater.*, 2013, **23**, 2714.
- K. Kanamori, K. Nakanishi, T. Hanada, *Adv. Mater.*, 2006, **18**, 2407.
- K. Kanamori, J. Hasegawa, K. Nakanishi, T. Hanada, *Macromolecules*, 2008, **41**, 7186.
- H. Sai, K. W. Tan, K. Hur, E. Asenath-Smith, R. Hovden, Y. Jiang, M. Riccio, D. A. Muller, V. Elser, L. A. Estroff, S. M. Gruner, U. Wiesner, *Science*, 2013, **341**, 530.
- K. Nakanishi, N. Tanaka, *Acc. Chem. Res.*, 2007, **40**, 863.
- N. Tarutani, Y. Tokudome, M. Fukui, K. Nakanishi, M. Takahashi, *RSC Adv.*, 2015, **5**, 57187.
- N. Moitra, K. Kanamori, Y. H. Ikuhara, X. Gao, G. Hasegawa, K. Takeda, Y. Zhu, T. Shimada, K. Nakanishi, *J. Mater. Chem. A*, 2014, **2**, 12535.
- H. Onoda, T. Yamaguchi, *Int. J. Cosmetic Sci.*, 2013, **35**, 196.
- A. Clearfield, D. S. Thakur, *Appl. Catal.*, 1986, **26**, 1.
- P. Cheng, T. Lan, W. Wang, H. Wu, H. Yang, C. Deng, X. Dai, S. Guo, *Sol. Energy*, 2010, **84**, 854.
- K. Takeda, *Rev. Sci. Instrum.*, 2007, **78**, 033103.
- K. Takeda, *J. Magn. Reson.*, 2008, **192**, 218.
- G. Guerrero, M. Mehrling, P. H. Mutin, F. Dahan, A. Vioux, *J. Chem. Soc., Dalton Trans.*, 1999, 1537.
- C. Santato, C. M. López, K. S. Choi, *Electrochem. Commun.*, 2007, **9**, 1519.
- G. Alberti, S. Masci, R. Vivani, *Inorg. Chem.*, 2002, **41**, 1913.
- Integrated Spectral Database System of Organic Compounds (National Institute of Advanced Industrial Science and Technology (Japan)), http://sdb.sdb.aist.go.jp/sdb/cgi-bin/direct_frame_top.cgi, (accessed November 2015).
- K. Nakamoto, *Infrared and Raman Spectra of Inorganic and Coordination Compounds*, 6th ed., Wiley-Interscience: New York, 2009.
- D. J. Jones, G. Aptel, M. Brandhorst, M. Jacqun, J. Jiménez-Jiménez, A. Jiménez-López, P. Maireles-Torres, I. Piwaonski, E. Rodríguez-Castellón, J. Zajac, J. Rozière, *J. Mater. Chem.*, 2000, **10**, 1957.
- Y. J. Li, M. S. Whittingham, *Solid State Ionics*, 1993, **391**, 63.
- Y. Berezniński, M. Jaroniec, A. I. Bortun, D. M. Poojary, A. Clearfield, *J. Colloid Interface Sci.*, 1997, **191**, 442.
- H. Nakayama, T. Eguchi, N. Nakamura, S. Yamaguchi, M. Danjyo, M. Tsuchioka, *J. Mater. Chem.*, 1997, **7**, 1063.
- Morse, J. W.; Arvidson, R. S.; Lüttge, A. *Chem. Rev.*, 2007, **107**, 342.

- 40 van Driessche, A. E. S.; Benning, L. G.; Rodriguez-Blanco, J. D.; Ossorio, M.; Bots, P.; Garcia-Ruiz, J. M. *Science*, 2012, **336**, 69.
- 41 A. Dey, P. H. Bomans, F. A. Müller, J. Will, P. M. Frederik, G. de With, N. A. Sommerdijk, *Nat. Mater.*, 2010, **9**, 1010.
- 42 S. Bach, V. R. Celinski, M. Dietzsch, M. Panthöfer, R. Bienert, F. Emmerling, J. S. auf der Günne, W. Tremel, *J. Am. Chem. Soc.*, 2015, **137**, 2285.

Table of contents entry



A new hierarchically porous titanium phosphate monolith is synthesized via sol-gel method and its crystallization in ethylene glycol is observed.